Biomimics of [FeFe]-hydrogenases with a pendant amine: diphosphine complexes [Fe2(CO)4{μ-S(CH 2)nS}{κ2-(Ph2PCH2)2NR}](n=2, 3; R=Me, Bn) towards H2 oxidation catalysts

Journal of Organometallic Chemistry 991 (2023) 122673

Contents lists available at ScienceDirect

Journal of Organometallic Chemistry

journal homepage: www.elsevier.com/locate/jorganchem

Biomimics of [FeFe]-hydrogenases with a pendant amine: Diphosphine complexes $[Fe_2(CO)_4\{\mu\text{-}S(CH_2)_nS\}\{\kappa^2\text{-}(Ph_2PCH_2)_2NR\}]$ (n = 2, 3; R = Me, Bn) towards H_2 oxidation catalysts

Georgia R.F. Orton[a], Sara Belazregue[a], Jeremy K. Cockcroft[b], František Hartl[c], Graeme Hogarth[a,*]

[a] Department of Chemistry, King's College London, 7 Trinity Street, London, SE1 1DB, UK
[b] Department of Chemistry, University College London, 20 Gordon Street, London, WC1H 0AJ, UK
[c] Department of Chemistry, University of Reading, Whiteknights, Reading RG6 6AD, UK

ARTICLE INFO

Article history:
Received 30 January 2023
Revised 27 February 2023
Accepted 4 March 2023
Available online 6 March 2023

Keywords:
Hydrogenase-biomimic
Amino-diphosphine
Proton-transfer
IR-SEC
H_2 oxidation

ABSTRACT

We report the synthesis and molecular structures of [FeFe]-ase biomimics $[Fe_2(CO)_4\{\mu\text{-}S(CH_2)_nS\}\{\kappa^2\text{-}(Ph_2PCH_2)_2NR\}]$ (**1–4**) (n = 2, 3; R = Me, Bn) and a comparative study of their protonation and redox chemistry, with the aim of assessing their activity as catalysts for H_2 oxidation. They are prepared in good yields upon heating the hexacarbonyls and PCNCP ligands in toluene, a minor product of one reaction (n = 3, R = Bn) being pentacarbonyl $[Fe_2(CO)_5(\mu\text{-pdt})\{Ph_2PCH_2N(H)Bn\}]$ (**5**). Crystal structures show short Fe-Fe bonds (ca. 2.54 Å) with the diphosphine occupying basal-apical sites. Each undergoes a quasi-reversible one-electron oxidation and IR-SEC shows that this results in formation of a semi-bridging carbonyl. As has previously been observed, protonation products are solvent dependent, nitrogen being the favoured site of protonation site upon addition of one equivalent of $HBF_4.Et_2O$ in d_6-acetone, while hydride formation is favoured in CD_2Cl_2. However, the rate of N to Fe_2 proton-transfer varies greatly with the nature of both the dithiolate-bridge and amine-substituent. Thus with NMe complexes (**1–2**) N-protonation is favoured in acetone affording a mixture of *endo* and *exo* isomers, while for NBn complexes (**3–4**) proton-transfer to afford the corresponding μ-hydride occurs in part (for **3** edt) or exclusively (for **4** pdt). In acetone, addition of a further equivalent of $HBF_4.Et_2O$ generally does not lead to hydride formation, but in CD_2Cl_2 dications $[Fe_2(CO)_4\{\mu\text{-}S(CH_2)_nS\}(\mu\text{-H})\{\kappa^2\text{-}(Ph_2PCH_2)_2NHR\}]^{2+}$ result, in which the diphosphine can adopt either dibasal or basal-apical positions. Proton-transfer from Fe_2 to N has been previously identified as a required transformation for H_2 oxidation, as has the accessibility of the all-terminal carbonyl isomer of cations $[Fe_2(CO)_4\{\mu\text{-}S(CH_2)_nS\}\{\kappa^2\text{-}(Ph_2PCH_2)_2NR\}]^+$. We have carried out a preliminary H_2 oxidation study of **3,** oxidation by $Fc[BF_4]$ in the presence of excess P(o-tolyl)$_3$ affording $[HP(o\text{-tol})_3][BF_4]$, with a turnover of ca. 2.3 ± 0.1 mol of H_2 consumed per mole of **3**

1. Introduction

Hydrogenases are ancient enzymes that efficiently catalyse the reduction of protons and oxidation of hydrogen [1]. While there are three types, the most prevalent and widely studied are the so-called [FeFe]-ases, the active site of which feature a diiron centre spanned by a bridging dithiolate group and supported by carbonyl and cyanide ligands, being linked to a [4Fe-4S] cluster *via* one of the thiolate groups (Chart 1a). Over the past 20 years there has been significant development of [FeFe]-ase biomimics [2] with diphosphine complexes of the type $[Fe_2(CO)_4(\mu\text{-dithiolate})(\kappa^2\text{-diphosphine})]$ (Chart 1b) being widely targeted [3] as the asymmetric introduction of strong donor ligands provides good structural and functional models [4].

A further feature of the active site of [FeFe]-ases (Chart 1a) is the presence of a central amine on the dithiolate ligand. This acts as a Lewis base, reversibly binding a proton, and transferring it to the electron-deficient Fe_2 centre. Consequently, the inclusion into [FeFe]-ase biomimics of an amine functionality able to act as a proton-relay, is desirable feature. This can best be achieved using an amino-dithiolate (adt) bridge [5], but a number of alternative ways have also been explored [6]. An attractive option is to

* Corresponding author.
E-mail address: graeme.hogarth@kcl.ac.uk (G. Hogarth).

https://doi.org/10.1016/j.jorganchem.2023.122673

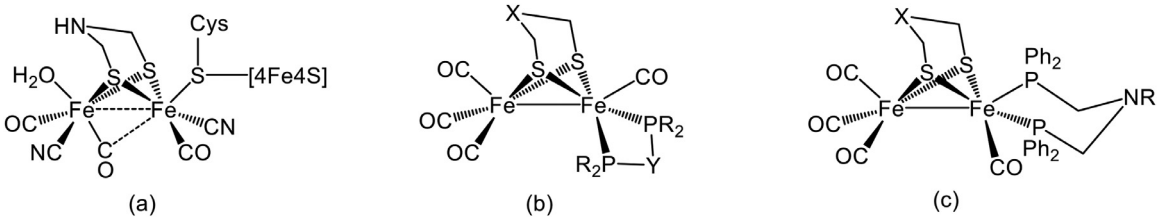

Chart 1. Line drawings of (a) the active site of [FeFe]-ases, (b) $[Fe_2(CO)_4(\mu\text{-dithiolate})(\kappa^2\text{-diphosphine})]$ in the dibasal form, (c) $[Fe_2(CO)_4(\mu\text{-dithiolate})\{\kappa^2\text{-}Ph_2PCH_2N(R)CH_2PPh_2\}]$ in the basal-apical form.

include the Lewis base into the chelating diphosphine, as in so-called PCNCP ligands, with generation of biomimics of the type $[Fe_2(CO)_4(\mu\text{-dithiolate})\{\kappa^2\text{-}Ph_2PCH_2N(R)CH_2PPh_2\}]$ (Chart 1c) [7–15]. A number of diiron PCNCP complexes have been prepared and protonation and oxidation studies carried out [7–13]. A key finding of these studies is that they catalyse the oxidation of H_2 [13], a challenging process for which only a small number of [FeFe]-ase biomimics have been shown to be active [16–18]. Herein we report three further examples of [FeFe]-ase biomimics containing PCNCP ligands with the aim of exploring their structural, oxidation and protonation chemistry, specifically to see if they are dependant upon the nature of the dithiolate backbone and substituent on nitrogen and also report another example of an [FeFe]-ase biomimic acting as a H_2 oxidation catalyst.

2. Results and discussion

2.1. Synthesis of $[Fe_2(CO)_4\{\mu\text{-}S(CH_2)_nS\}\{\kappa^2\text{-}(Ph_2PCH_2)_2NR\}]$ (1–4) (n = 2, 3; r = me, bn) and $[Fe_2(CO)_5(\mu\text{-pdt})\{Ph_2PCH_2N(H)Bn\}]$ (5)

PCNCP ligands, $(Ph_2PCH_2)NMe$ and $(Ph_2PCH_2)NBn$, were prepared following literature procedures [19]. Reaction of either $[Fe_2(CO)_6(\mu\text{-edt})]$ or $[Fe_2(CO)_6(\mu\text{-pdt})]$ with one equivalent of diphosphine in refluxing toluene afforded $[Fe_2(CO)_4\{\mu\text{-}S(CH_2)_nS\}\{\kappa^2\text{-}(Ph_2PCH_2)_2NR\}]$ (**1–4**) as brown microcrystalline solids following purification (Scheme 1) Complex **2** has previously been reported and our preparation follows that in the literature [8].

All were characterised by IR, ^1H and $^{31}P\{^1H\}$ NMR spectroscopy, mass spectrometry and elemental analysis. Spectroscopic data (see experimental section) are similar to those reported for other diiron PCNCP complexes of this type and do not warrant detailed consideration [8]. During the purification of **4**, a small amount of a red by-product was isolated being identified as $[Fe_2(CO)_5(\mu\text{-pdt})\{Ph_2PCH_2N(H)Bn\}]$ (**5**). Similar faint red bands were observed upon purification of **1** and **3**, however, these faded on columns and were not collected. Although the PCNCP ligands were not extensively purified prior to use, $^{31}P\{^1H\}$ NMR spectroscopy revealed that they contained only trace amounts of $(Ph_2PCH_2)N(H)R$, and thus **5** likely results from hydrolysis of the PCNCP ligand under the reaction conditions employed.

2.2. Molecular structures

Molecular structures of **1, 3** and **4**.CH_2Cl_2 were obtained from crystals grown in CH_2Cl_2:hexane solutions at 5 °C (Fig. 1). In 1, 3–4, the diphosphine occupies an apical-basal position as seen in other complexes of this type [8–12] with bite angles of 91–94° and Fe-Fe bond lengths of ca. 2.52–2.57 Å are also consistent with the short Fe-Fe distances seen in others (Table 1). The PCNCP bite angles range between 91–93° being comparable to that in **2** and other related complexes (Table 1).

Table 1
Fe-Fe bond lengths (Å) and P-Fe-P bond angles (°) for 1–5 and related PCNCP complexes.

Complex	Fe-Fe	PCNCP	Ref
1	2.5238(4)	91.3520(8)	this work
2	2.5687(7)	94.05(4)	8
3	2.5395(4)	93.027(4)	this work
4	2.5424(4)	91.304(3)	this work
R = Pr, pdt	2.5564(7)	92.51(4)	9
R = Ph, pdt	2.576(2)	94.39(12)	10
R = Bu^i, pdt	2.5556(11)	93.03(6)	11
R = Pr, edt	2.5618(7)	92.99(3)	12
R = Bu^t, edt	2.5495(6)	93.21(3)	11
R = Bu^n, edt	2.5473(10)	93.44(5)	11
$Fe_2(CO)_4(\mu\text{-pdt})(\kappa^2\text{-dppp})$	2.5614(3)	94.96(2)	9
5	2.5122(3)	-	this work

The molecular structure of **5** is shown (Fig. 2). It is generally unremarkable and has metric features similar to related complexes of the type $[Fe_2(CO)_5(\mu\text{-pdt})(Ph_2PR)]$ [20] and $[Fe_2(CO)_5(\mu\text{-dithiolate})(Ph_2PNR)]$ [21]. Thus, the phosphine adopts an apical position, lying approximately *trans* to the Fe-Fe bond which is slightly (but not substantially) shorter than those in the PCNCP complexes (Table 1).

2.3. Oxidation chemistry: cyclic voltammetry and IR-spectroelectrochemistry

Earlier work has shown that $[Fe_2(CO)_4(\mu\text{-dithiolate})\{\kappa^2\text{-}(Ph_2PCH_2)_2N(R)\}]$ complexes undergo a reversible metal-based one electron oxidation at low potentials resulting in formation of a cation [9–13]. As confirmed in the molecular structure of $[Fe_2(CO)_4(\mu\text{-pdt})\{\kappa^2\text{-}(Ph_2PCH_2)_2N(Pr)\}][BAr^F{}_4]$ [13], there are two significant structural changes upon oxidation, (i) one of the carbonyls moves from a terminal to semi-bridging position and (ii) the diphosphine rotates into a (pseudo) dibasal position (Scheme 2). This geometric change is important with respect to H_2 oxidation as DFT calculations have shown that the thermodynamically favoured semi-bridged isomer is unable to activate H_2 [13–15] and thus changing the energy of this

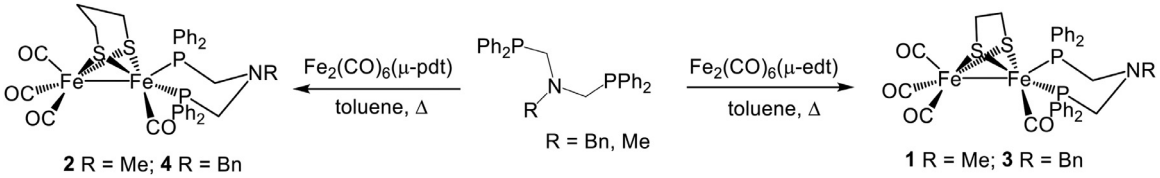

Scheme 1. Synthesis of $[Fe_2(CO)_4(\mu\text{-dithiolate})\{\kappa^2\text{-}(Ph_2PCH_2)_2N(R)\}]$ (**1–4**).

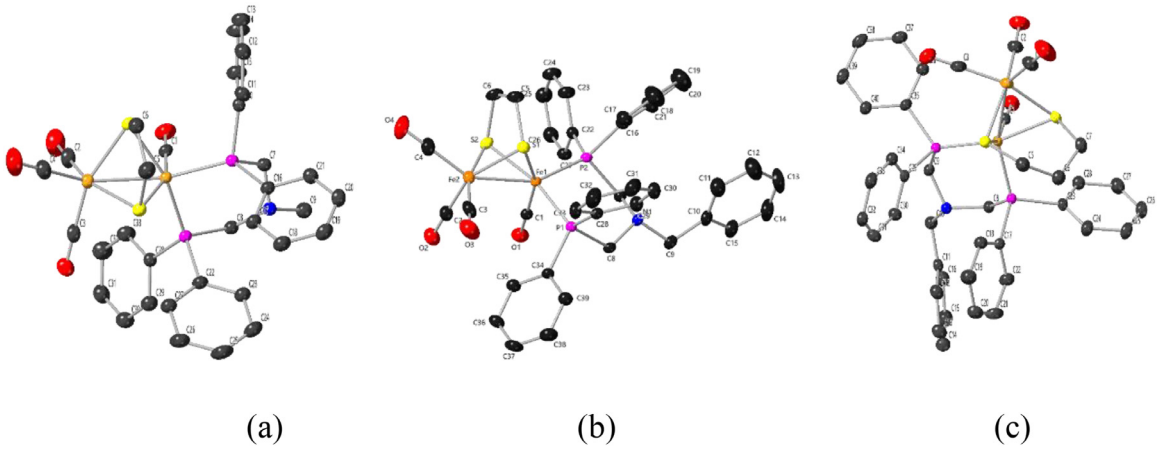

Fig. 1. Molecular structures of (a) 1, (b) 3 and (c) 4 with thermal ellipsoids shown at 50% probability and hydrogen atoms omitted for clarity.

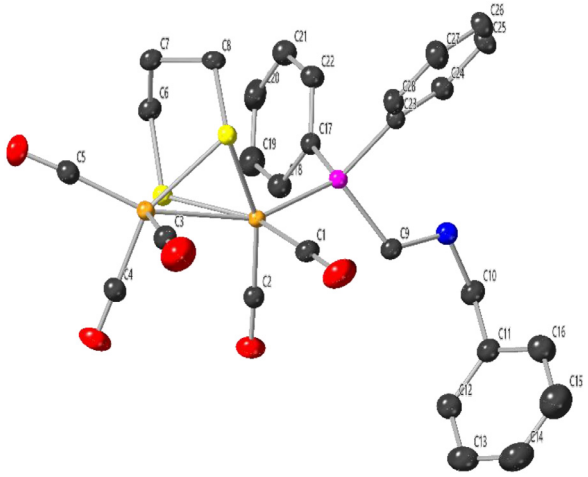

Fig. 2. Crystal structure of 5 with thermal ellipsoids shown at 50% probability and hydrogen atoms omitted for clarity.

isomerisation is important in H_2 activation. Sun, Ahlquist and co-workers have studied isomerisation of $[Fe_2(CO)_4(\mu\text{-pdt})\{\kappa^2\text{-}Ph_2PCH_2N(Pr)CH_2PPh_2\}]^+$ by DFT, finding a free energy barrier of 14.6 kcal mol^{-1} for CO rotation [13].

Complexes **1** (**Fig. S1**) and **3–4** (Fig. 3) each undergo a one electron oxidation at −0.14 V ($\Delta E_{1/2}$ = 190 mV), −0.16 V ($\Delta E_{1/2}$ = 450 mV), and −0.16 V ($\Delta E_{1/2}$ = 130 mV) vs. $Fc^{+/0}$ respectively, whilst **2** has previously been reported to undergo oxidation at −0.05 V under similar conditions [8]. Oxidation of **3** is quasi-reversible and appears to be unaffected by scan rate over the range investigated, however, two return reduction waves are associated with oxidation **4**, being accompanied by a significantly larger ΔE. Two reduction waves are also associated with oxidation of **1**, although the secondary wave at more negative potentials is much less pronounced than for **4**. Thus, while oxidation potentials of edt and pdt analogues are generally similar, the significant difference in $\Delta E_{1/2}$ suggests that associated geometric rearrangements occur at different rates. Sun and co-workers have previously compared edt [12] and pdt [13] derivatives of the n-propyl complex, noting quite different behaviour. Thus, oxidation of the edt complex (−0.11 V) is easier than the pdt (−0.22 V) but their reversibility is similar.

We next studied the oxidation of **3** by IR-SEC (Fig. 4a), the ca. 60 cm^{-1} hypsochromic shift in the ν(CO) bands being indicative of formation of a semi-bridging carbonyl absorption. We were unable to observe an all-terminal carbonyl isomer spectroscopically, likely due to the slower timescale of IR-SEC as compared to CV and because the lowest frequency IR band for the all-terminal species would be hidden under the central IR band for the neutral species. We suggest that the two reduction waves observed in the CV for **4** are associated with reduction of an all-terminal and semi-bridging oxidation products, the latter persisting in solution and detectable by IR-SEC. It is expected that both steric congestion and bridgehead flexibility will both influence the rate of geometric rearrangement necessary for formation of a semi-bridging carbonyl and (consequently) generation of a vacant coordination site. We were unable to obtain good quality IR-SEC data for **4** as oxidation results in passivation of the Pt mini-grid OTTLE cell electrode. We thus chemically oxidised it using $Fc[BF_4]$ to give a near-identical IR spectrum (Fig. 4b) to those obtained for the cations $\mathbf{1}^+$–$\mathbf{2}^+$ (**Fig. S2**). These results show that generation of a vacant coordination site is dependent on the relatively slow rearrangement of the cation to a rearranged species with a semi-bridging CO and may be the rate-determining step for catalytic H_2 oxidation.

2.4. Protonation studies with $HBF_4.Et_2O$

As detailed earlier, the protonation-deprotonation chemistry of $[Fe_2(CO)_4(\mu\text{-pdt})\{\kappa^2\text{-}Ph_2PCH_2N(Me)CH_2PPh_2\}]$ (**2**) has been previously studied and is summarised in Scheme 3 [8]. Addition of one equivalent of $HBF_4.Et_2O$ in acetone affords predominantly (ca. 84:16) the N-protonated product, $[Fe_2(CO)_4(\mu$-

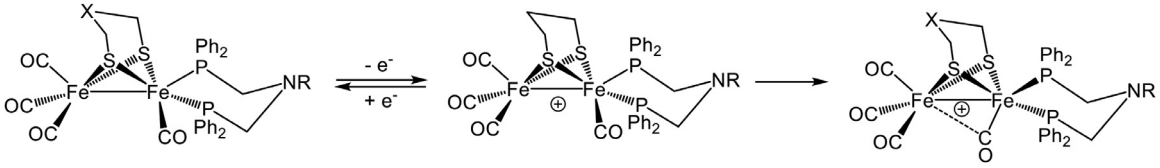

Scheme 2. Oxidation of $[Fe_2(CO)_4(\mu\text{-dithiolate})\{\kappa^2\text{-}(Ph_2PCH_2)_2N(R)\}]$ to afford kinetically favoured all terminal CO cation which isomerises to thermodynamically favoured semi-bridging carbonyl.

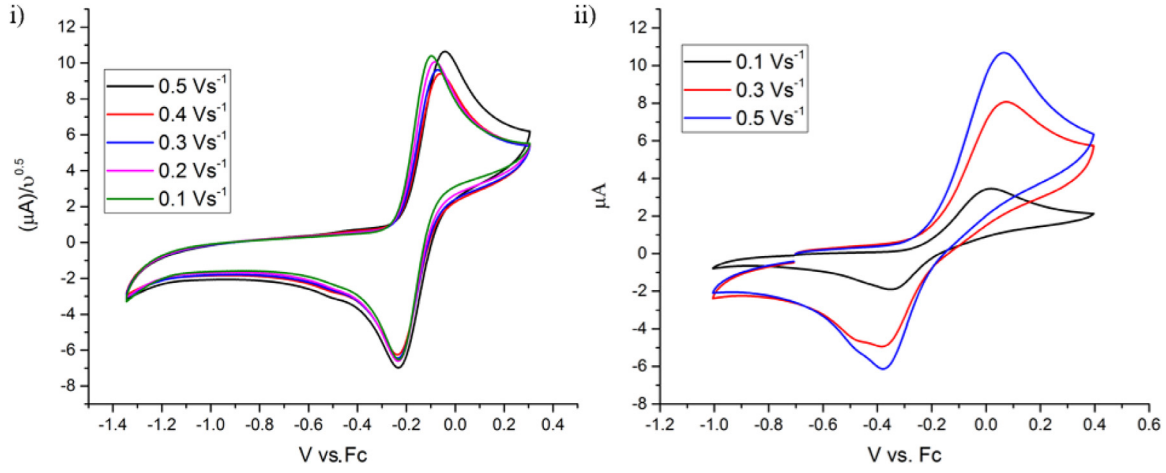

Fig. 3. CVs (1 mM solution in 0.1 M TBAFP/CH_2Cl_2) of (i) 3 (normalised for scan rate), and (ii) 4 at varying scan rates.

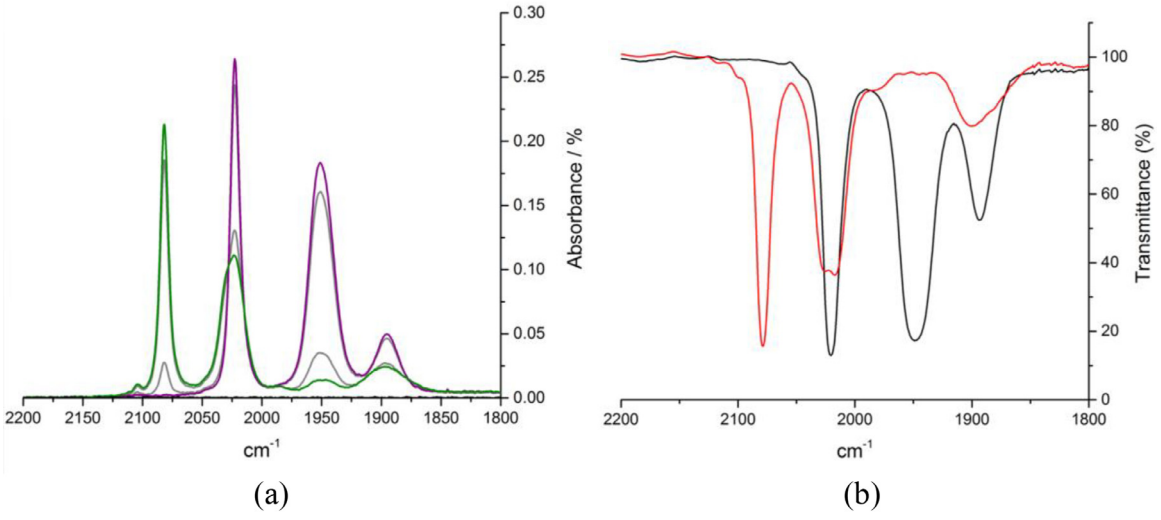

Fig. 4. (a) IR SEC of a 1 mM solution of **3** in 0.1 M TBAFP/ CH_2Cl_2 (purple = **3**, green = $\mathbf{3}^+$); (b) chemical oxidation of **4** in CH_2Cl_2 (black = **4**, red = $\mathbf{4}^+$). In (a) grey lines represent scans at intermediate points where multiple species exist in the solution.

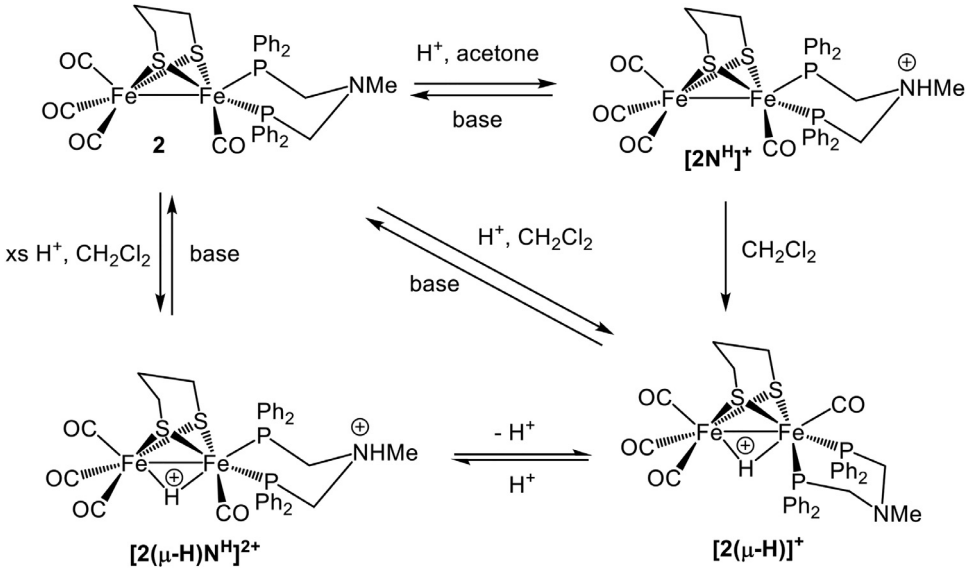

Scheme 3. Protonation chemistry of 2 with $HBF_4.Et_2O$ in CH_2Cl_2 and acetone [8].

pdt){κ^2-(Ph_2PCH_2)$_2$N(H)Me}]$^+$ [**2N^H**][BF_4] (as a mixture of *exo* and *endo* isomers), together with smaller amounts of bridging-hydride [Fe_2(μ-H)(CO)$_4$(μ-pdt){κ^2-(Ph_2PCH_2)$_2$NMe}][BF_4] [**2(μ-H)**][BF_4]. Further, the former isomerises cleanly to the latter in CH_2Cl_2, and can also be formed directly in this solvent [8]. Addition of excess HBF_4.Et_2O to [**2N^H**][BF_4] in acetone does not give any further protonation, but in CH_2Cl_2 the doubly protonated species [Fe_2(μ-H)(CO)$_4$(μ-pdt){κ^2-(Ph_2PCH_2)$_2$N(H)Me}][BF_4]$_2$ [**2(μ-H)N^H**][BF_4]$_2$ is formed. Importantly, and in contrast to the related 1,3-bis(diphenylphosphino)propane (dppp) complex [13], addition of aniline leads to regeneration of **2**, a process which is vital for catalytic H_2 oxidation [16]. To further establish whether this general scheme is ligand dependent, we have studied the protonation behaviour of **1** and **3–4** in both CD_2Cl_2 and d_6-acetone by ^{1}H and ^{31}P{^{1}H} NMR spectroscopy.

We first considered **1**, expecting that as the basicity and (broadly) steric nature of the diiron and nitrogen centres do not significantly differ from **2**, that it would behave in the same way. In acetone this is the case, addition of one equivalent of HBF_4.Et_2O to **1** affording [**1N^H**][BF_4], the presence of *endo* and *exo* isomers being apparent via two singlets (ratio ca. 10:1) in the ^{31}P{^{1}H} NMR spectrum (**Fig. S3**) [8]. No further changes were noted upon addition of more HBF_4.Et_2O, which is also in-line with observations for **2**. In CD_2Cl_2, addition of one equivalent of HBF_4.Et_2O gave an immediate colour change from green to red-brown and a shift in the ^{31}P{^{1}H} NMR spectrum of the singlet for **1** (53.3 ppm) to 58.2 ppm, consistent with amine protonation to form [**1N^H**][BF_4] (**Fig. S4**) (being assumed to be the *endo* isomer). This is in marked contrast to **2** (and also **3** – see later) and no evidence of hydride formation was noted. Thus, the expected proton-transfer between N and Fe_2 centres is far slower for **1** than **2,** something that has repercussions for H_2 activation as the reverse Fe_2 to N transfer is a key requirement [13–15]. However, addition of a further equivalent of HBF_4.Et_2O resulted in the concomitant appearance of a singlet at 45.5 ppm in the ^{31}P{^{1}H} NMR and a resonance at δ −16.0 in the ^{1}H NMR spectrum, being consistent with the formation of proton-hydride [**1(μ-H)N^H**][BF_4]$_2$. Given the slow N to Fe_2 proton-transfer noted above, this suggests that the second protonation of **1** i.e. protonation of [**1N^H**][BF_4] occurs directly at the Fe_2 centre. Thus, while gross features of the protonation of NMe complexes **1** and **2** appear similar, there is a marked difference in the rate of N to Fe_2 proton-transfer, being much faster for **2** (pdt) than **1** (edt).

We then considered if this was a general effect by studying the protonation of edt-NBn derivative **3**. In acetone the behaviour was similar to that of **1**, addition of one equivalent of HBF_4.Et_2O affords *endo* and *exo* isomers of [Fe_2(CO)$_4$(μ-edt){κ^2-(Ph_2PCH_2)$_2$N(H)Bn}][BF_4] [**3N^H**][BF_4] as the major product (**Fig. S5**) although now a small amount of Fe_2 protonated [**3(μ-H)**][BF_4] was observed, as evidenced by a low-intensity high field triplet at δ −15.6 (J_{PH} = 18.5 Hz) in the ^{1}H NMR spectrum and a ^{31}P{^{1}H} NMR signal at 39.4 ppm. Unexpectedly, and different to the behaviour of both **1** and **2**, addition of a second equivalent of HBF_4.Et_2O in acetone resulted in formation of a small amount of doubly-protonated [**3(μ-H)N^H**][BF_4]$_2$. Unfortunately, we have been unable to ascertain whether this results from N to Fe_2 proton-transfer or direct protonation of the Fe_2 centre. In CD_2Cl_2, addition of HBF_4.Et_2O to **3** (**Fig. S6**) results in the replacement of the ^{31}P NMR signal (at 53.8 ppm) with a singlet at 40.2 ppm and two small doublets at 45.9 and 38.7 (J_{PP} = 57.8 Hz) ppm. These new peaks are associated with dibasal and basal-apical isomers respectively of the bridging hydride [Fe_2(CO)$_4$(μ-H)(μ-edt){κ^2-(Ph_2PCH_2)$_2$NBn}][BF_4] [**3(μ-H)**][BF_4] [7] and are associated with hydride resonances at δ −15.5 (t, J_{PH} = 18.1 Hz, dibasal) and δ −16.8 (dd, J_{PH} = 22.2, 5.2 Hz, basal-apical) in the ^{1}H NMR spectrum. Thus, hydride formation is associated with movement of the diphosphine from an apical-basal to a dibasal site (kinetic product), the latter converting to the thermodynamically favoured apical-basal isomer (Scheme 4). This behaviour while akin to that seen for **2** [8] is quite different from that of **1** showing that the rate of N to Fe_2 transfer is also highly dependent upon the substituent at nitrogen. Addition of a second equivalent of HBF_4.Et_2O results in formation of doubly protonated [Fe_2(CO)$_4$(μ-H)(μ-edt){κ^2-(Ph_2PCH_2)$_2$N(H)Bn}][BF_4] [**3(μ-H)N^H**][BF_4]$_2$, as evidenced by a new signal at 47.3 ppm in the ^{31}P{^{1}H} NMR spectrum. In the ^{1}H NMR spectrum, the hydride region was broad and complex, which could result from an equilibrium between mono- and di-protonated forms that lies towards the latter, although we have no direct evidence to confirm this.

Unlike complexes **1–3**, protonation of **4** with one equivalent of HBF_4.Et_2O in acetone (**Fig. S7**) results in the unexpected formation of bridging hydride [**4(μ-H)**][BF_4] rather than [**4N^H**][BF_4], the hydride appearing as a triplet at δ −13.1 (J_{PH} 18.2 Hz) confirming a dibasal coordination of the diphosphine. Further, upon addition of a second equivalent of HBF_4.Et_2O only a small amount of [**4(μ-H)N^H**][BF_4]$_2$ is produced. It is not clear why such a marked difference in reactivity should occur between **1–3** and **4** but highlights the fine balance that exists in these systems. In CD_2Cl_2 **4** exhibits very similar protonation behaviour to that in acetone, being akin to that found for **3** in this solvent: with one equivalent of HBF_4, hydride [**4(μ-H)**][BF_4] is formed, while addition of a second equivalent (**Fig. S8**) gives [**4(μ-H)N^H**][BF_4]$_2$. Spectra are broader in CD_2Cl_2 suggesting that a small excess of acid may have been inadvertently added. Changes can be tracked by ^{31}P{^{1}H} NMR spectroscopy (especially that in d_6-acetone), the initial signal at 53.0 ppm being replaced by a singlet at 38.0 ppm, which is then shifted to 46.4 ppm upon addition of the second equivalent, and in the ^{1}H NMR, broad hydride signals appear at δ −13.1 for the singly protonated species and δ −13.9 for the doubly protonated species. Thus, unlike **3** only the dibasal isomer of [**3(μ-H)**][BF_4] is produced and we did not observe any rearrangement to the basal-apical isomer (Scheme 4). This suggests that either the dibasal isomer is thermodynamically favoured or possibly as a result of the increased steric bulk at the bridgehead, the isomerisation energy is too high. We favour the latter but have not been able to unequivocally differentiate between the two possible explanations.

Thus, while the protonation behaviour of complexes of the type [Fe_2(CO)$_4$(μ-dithiolate){κ^2-$Ph_2PCH_2N(R)CH_2PPh_2$}] is broadly represented by that of **2** (Scheme 4), there are small, and sometimes significant differences between **1–4**, notably in the formation of dibasal and basal-apical isomers of hydride-bridged mono-cations and the relative amounts of N-protonation products generated in acetone. Most noteworthy is the clean formation of N-protonated [**1N^H**][BF_4] upon addition of one equivalent of HBF_4.Et_2O to **1** in acetone, while under the same conditions **4** exclusively affords hydride-bridged [**4(μ-H)**][BF_4]. This suggests that small differences in the pK_b, the steric accessibility of diiron and amine centres, and diphosphine rearrangement energies can be affected by making changes to both the dithiolate bridge and nitrogen-substituent, which in turn can lead to different rates of protonation (and deprotonation) relevant to their ability to act as H_2 oxidation and proton-reduction catalysts.

2.5. Hydrogen oxidation

As detailed in the introduction, in 2013, Sun and co-workers reported that [Fe_2(CO)$_4$(μ-H)(μ-pdt){κ^2-(PPh_2CH_2)$_2$N(H)Pr}][BF_4] was catalytically active for H_2 oxidation with a turnover of 6.2 ± 0.1 mol of H_2 consumed per mole of catalyst [13]. Ahlquist and co-workers [13–15] have investigated this process using DFT calculations, a simplified version of which is shown in Scheme 5. Key features are: (i) the conversion of the thermodynamically favoured cation with a semi-bridging carbonyl into one with a dibasal diphosphine and an all-terminal arrangement of the carbonyls, (ii)

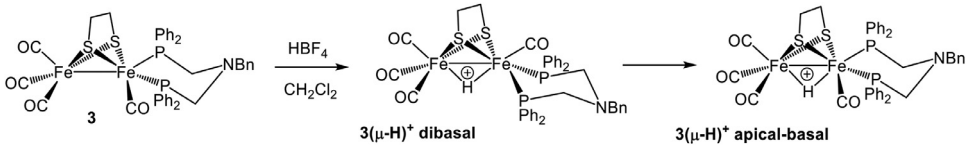

Scheme 4. Formation of dibasal [**3(μ-H)**]$^+$ and isomerisation to the thermodynamically favoured apical-basal isomer.

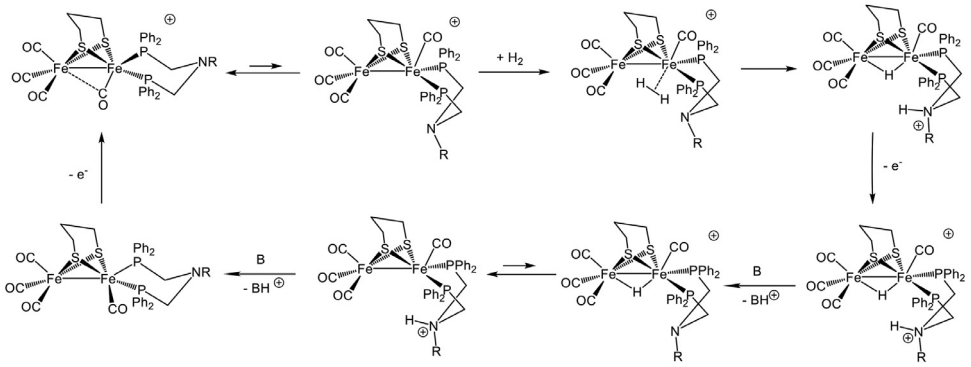

Scheme 5. Simplified version of the H_2 oxidation mechanism (R = Pr) proposed by Ahlquist and co-workers [13–15].

binding of H_2 and heterolytic cleavage to give a hydride and an N-bound proton, (iii) removal of the latter by external base, (iv) transfer of the hydride to the nitrogen, (v) subsequent deprotonation to regenerate the catalyst.

The rate-limiting step is the conversion of the semi-bridging to all-carbonyl cation, being calculated to have an energy barrier of 14.6 kcal mol^{-1} (R = Pr, pdt) [13]. This suggested to us that other diiron PCNCP complexes may have higher activity and we tested this by reproducing the conditions of Sun but using **3** as the pre-catalyst. Thus, a sample of **3** was dissolved in CD_2Cl_2 and degassed with H_2 before addition of ca. 9 equivalents of Fc[BF_4], in order to generate the active **3**$^+$ and 9 equivalents of P(o-tolyl)$_3$ as a proton-abstraction agent. The combined sample was transferred to an NMR tube, the headspace filled with H_2 (1 atm), and conversion of P(o-tolyl)$_3$ to [HP(o-tolyl)$_3$]$^+$ monitored by $^{31}P\{^1H\}$ NMR spectroscopy. A series of spectra were recorded (**Fig. S9**) and after 3 h showed ca. 50% conversion of P(o-tol)$_3$ to [HP(o-tol)$_3$][BF_4], indicating that **3**$^+$ can oxidise H_2 although the turnover of ca. 2.3 ± 0.1 mol of H_2 consumed per mole of **3** is lower than that found for [$Fe_2(CO)_4$(μ-H)(μ-pdt){κ^2-(PPh_2CH_2)$_2$NPr}] [13].

3. Summary and conclusions

In this contribution we have extended the number of diiron PCNCP complexes of the type [$Fe_2(CO)_4${μ-S(CH_2)$_n$S}{κ^2-(Ph_2PCH_2)$_2$NR}] preparing and crystallographically characterising three new examples. All have the same ground state features as those previously prepared, containing a short Fe-Fe contact with the diphosphine occupying apical-basal sites. One electron oxidation, either chemically or by cyclic voltammetry, affords cations with a semi-bridging carbonyl as can be clearly seen in their IR spectra. IR-SEC gives similar results and we have been unable to spectroscopically detect the all-terminal isomers, although some evidence for their existence comes from CV studies. We have studied their protonation with HBF_4.Et_2O in both d_6-acetone and CD_2Cl_2. Initial proton addition occurs at the N-centre and in acetone this is often the final product, existing as *exo* and *endo* isomers. Proton-transfer can also occur to afford the isomeric μ-hydride which tends to be much faster in CD_2Cl_2 than acetone, but rates also vary significantly are broadly similar but do vary depending upon both the nature of the amine-substituent and dithiolate backbone. This is important as the reverse proton-transfer, from Fe_2 to N is a key step in the catalytic H_2 oxidation cycle. On the basis of CV and protonation measurements we chose to study **3** as a catalyst for H_2 oxidation using Fc[BF_4] as the oxidant and P(o-tolyl)$_3$ as the proton-acceptor. The system is catalytically active but the estimated turnover of 2.3 ± 0.1 mol of H_2 consumed per mole of **3** is lower than that found for [$Fe_2(CO)_4$(μ-H)(μ-pdt){κ^2-(PPh_2CH_2)$_2$NPr}] by Sun and co-workers [13].

4. Experimental section

4.1. General

All reactions were carried out using standard Schlenk-line techniques under N_2 using anhydrous solvents. Work-up was done in air using standard bench reagents. NMR spectra were recorded on a BrukerAvance 400 MHz Ultrashield NMR spectrometer and referenced internally to residual solvent peaks or to the accepted standard (85% H_3PO_4) using the external resonance of P(OMe)$_3$. High resolution electron spray ionisation mass spectra were recorded on a Bruker Daltronics Esquire 3000 spectrometer by Dr Lisa Haigh (Imperial College). Fourier transform infrared (FTIR) spectra were recorded with a IRAffinity-1S Shimadzu spectrophotometer in a solution cell fitted with calcium fluoride plates, subtraction of the solvent absorptions being achieved by computation. Elemental analyses were carried out at London Metropolitan University. Diiron complexes [$Fe_2(CO)_6$(μ-edt)] and [$Fe_2(CO)_6$(μ-pdt)] [22] and diphosphines ($Ph_2P_2CH_2$)$_2$NBn and (Ph_2PCH_2)$_2$NMe [19] were synthesised according to literature procedures and stored as 2 M solutions in MeCN.

4.2. CV and IR-SEC

Electrochemistry was carried out in anhydrous degassed acetonitrile or dichloromethane solutions using 0.1 M TBAFP as the supporting electrolyte. Unless otherwise stated, the working electrode was a 3 mm diameter glassy carbon electrode that was polished with diamond slurry. The counter electrode was a Pt wire and the quasi-reference electrode was a silver wire or Pt electrode. All CVs were referenced to the Fc $^{+/0}$ or Fc$^{*+/0}$ redox couples. An Autolab Interface.6 potentiostat was used for electrochemical measurements. Proton reduction studies were carried out by adding equivalents of HBF_4.Et_2O (Sigma-Aldrich) which was used

as supplied. IR SEC was performed with a Bruker Vertex 70v FT-IR spectrometer equipped with a DTLaGS detector. The spectroelectrochemical experiment was recorded using thin-layer cyclic voltammetry (TL-CV) with an OTTLE cell, an EmStat3+ (PalmSens) potentiostat and the PSTrace 4.2 software. The OTTLE cell was equipped with a Pt minigrid-working electrode, a platinum minigrid counter electrode, an Ag-wire pseudo-reference electrode and CaF2 windows. SEC samples contained 0.3 M supporting electrolyte and 1 mM analyte.

4.3. X-Ray diffraction

X-ray diffraction data were collected at 150(1) K using an Agilent Oxford Diffraction SuperNova (equipped with a microfocus Cu Kα X-ray source, a Cryojet5®, and an Atlas CCD detector) using the CrysAlisPro software at University College London. The crystal structures of were solved using SHELXT [23,24] and refined using SHELXL [23] both of which were operated from within either the Oscail [25] or 4 [26] software packages. Important crystallographic data are given in **Table S1**. Crystallographic data were deposited with the Cambridge Data Centre with deposition numbers (see **Table S1**).

4.4. Synthesis

4.4.1. $[Fe_2(CO)_4(\mu\text{-edt})\{\kappa^2\text{-}(Ph_2PCH_2)_2NMe)\}]$ (**1**)

To a solution of $[Fe_2(CO)_6(\mu\text{-edt})]$ (250 mg, 0.67 mmol) in toluene (10 ml) was added $(Ph_2PCH_2)_2NMe$ (0.30 g, 0.74 mmol, 2 M MeCN solution). The solution was refluxed for 2.5 d under N_2. The solvent was removed under reduced pressure and the oily residue subjected to a 20 cm long silica gel column. Unreacted hexacarbonyl was eluted in hexane before obtaining the product as a dark green fraction from hexane- CH_2Cl_2 (5:1). The pure product was extracted from a trace amount of an unidentified red oily residue by crystallisation from CH_2Cl_2-hexane to give **1** (230 mg, 0.31 mmol, 46%) as a brown crystalline solid. ^1H NMR (CD_2Cl_2) δ 7.64 – 7.24 (20H, Ph), 3.66 (m, 2H, CH_2P) 3.06 (m, 2H, CH_2P), 2.38 (s, 3H, Me), 1.82 (m, 2H, CH_2), 1.66 (m, 2H, CH_2). $^{31}P\{^1H\}$ NMR (CD_2Cl_2) 53.3 ppm. IR (CH_2Cl_2) ν(CO): 2022 vs, 1950s, 1894 br cm^{-1}. ESI(+)MS: *m/z* calcd for ($C_{33}H_{31}Fe_2NO_4P_2S_2$)**:** 742.99; found 743.9957 [M+H$^+$]. Elemental analysis calcd (found) for $Fe_2S_2P_2N_1O_4C_{33}H_{31}$% C 53.30 (53.53), H 4.17 (4.19), N 1.88 (1.82).

4.4.2. $[Fe_2(CO)_4(\mu\text{-edt})\{\kappa^2\text{-}(Ph_2PCH_2\}_2NBn)\}]$(**3**)

To a solution of $[Fe_2(CO)_6(\mu\text{-edt})]$ (400 mg, 1.1 mmol) in toluene (10 ml) was added $(Ph_2PCH_2)_2NBn$ (0.60 g, 1.2 mmol) in MeCN. The solution was refluxed for 2 d under N_2. The solvent was removed under reduced pressure and the oily residue subjected to a 20 cm long silica gel column. The first fraction, a light orange band of the unreacted hexacarbonyl, was eluted in hexane before obtaining the product as a dark green fraction from hexane: CH_2Cl_2 (5:1). The pure product was extracted from a trace amount of an unidentified red oily residue by crystallisation from CH_2Cl_2-hexane to give **3** (160 mg, 0.2 mmol, 18 %) as a brown crystalline solid. ^1H NMR (CD_2Cl_2) δ 7.62–6.79 (m, 25H, Ph), 3.76 (m, 2H, NCH_2P), 3.61 (s, 2H, NCH_2Ph), 3.12 (m, 2H, NCH_2P), 1.80 (m, 2H, CH_2), 1.67 (m, 2H, CH_2). $^{31}P\{^1H\}$ NMR ($CDCl_3$) 53.8 ppm. ν(CO) 2023, 1950, 1895 cm^{-1}. ESI(+)MS: *m/z* calcd for ($C_{39}H_{35}Fe_2NO_4P_2S_2$): 819.02; found 819.0231. Elemental analysis calcd (found) for $Fe_2S_2P_2N_1O_4C_{39}H_{35}$% C 57.14 (56.80), H 4.27 (4.16), N 1.71 (1.64).

4.4.3. $[Fe_2(CO)_4(\mu\text{-pdt})\{\kappa^2\text{-}(Ph_2PCH_2)_2NBn)\}]$(4)

To a solution of $[Fe_2(CO)_6(\mu\text{-pdt})]$ (400 mg, 1.0 mmol) in toluene (10 ml) was added $(Ph_2PCH_2)_2NBn$ (0.60 g, 1.3 mmol) as a 2 M MeCN solution. The solution was refluxed for 1 d under N_2. The solvent was removed under reduced pressure and the oily residue subjected to a 20 cm long silica gel column. The first fraction, a light orange band of the unreacted hexacarbonyl, was eluted in hexane before obtaining the product as a wide brown fraction from hexane: CH_2Cl_2 (5:1). Crystallisation of the resulting brown solid from CH_2Cl_2-hexane gave **4** (145 mg, 0.17 mmol, 17%) as a brown crystalline solid. ^1H NMR (CD_2Cl_2) δ 7.70–6.81 (m, 25H, Ph), 3.82 (m, 2H, NCH_2P), 3.60 (s, 2H, NCH_2Ph), 3.22 (m, 2H, NCH_2P), 1.75 –1.39 (m, 6H, CH_2). $^{31}P\{^1H\}$ NMR ($CDCl_3$) 53.0 ppm. IR (CH_2Cl_2) ν(CO): 2020 (s), 1947 (br), 1893 cm^{-1}. ESI(+)MS: *m/z* calcd for ($C_{40}H_{37}Fe_2NO_4P_2S_2$): 833.03; Found: 833.0350 (M^+), 834.0415 ($M + H^+$). Elemental analysis calcd (found) for $Fe_2S_2P_2N_1O_4C_{40}H_{37}$% C 57.62 (57.51), H 4.44 (4.35), N 1.68 (1.63).

4.4.4. $[Fe_2(CO)_5(\mu\text{-pdt})\{\kappa^1\text{-}(Ph_2PCH_2)NH(Bn)\}]$ (**5**)

Following crystallisation of **4**, an oily red liquid remained in the vial. Storage in the freezer for 3 months resulted in the formation of dark red crystals of **5** (38 mg). ^1H NMR (CD_2Cl_2) δ 7.78 (m, 4H, Ph), 7.49 (m, 6H, Ph), 7.30 (m, 5H, Ph), 3.90 (s, 2H, CH_2Ph), 3.75 (d, J_{PH} 3 Hz, CH_2PPh_2), 1.84 – 1.54 (m, 6H, CH_2). $^{31}P\{^1H\}$ NMR ($CDCl_3$) 56.7 ppm. ESI(+)MS: *m/z* calcd for ($C_{28}H_{26}Fe_2NO_5PS_2$): 662.97; found 663.9733 [$M + H^+$]. IR (CH_2Cl_2) ν(CO): 2048 (s), 1987 (vs), 1967 (m) 1940 (w), 1929 (w) cm^{-1}. Elemental analysis calcd (found) for $Fe_2S_2P_1N_1O_5C_{28}H_{26}$% C 50.60 (50.37), H 3.88 (4.16), N 2.11 (2.08).

4.5. Protonation reactions

All protonation reactions were carried out in a standard NMR tube. Following dissolution of an appropriate amount of complex in the deuterated solvent, ^1H and $^{31}P\{^1H\}$ NMR spectra were recorded. Following this, 1–2 equivalent of the requisite acid was added using a micro-syringe and following shaking and allowing sample to equilibrate for ca. 5 min, both spectra were re-recorded. No attempts were made to isolate products. Selected NMR data; [**1N^H**]$^+$ $^{31}P\{^1H\}$ NMR (d_6-acetone) 58.2 & 57.9 ppm, $^{31}P\{^1H\}$ NMR (CD_2Cl_2) 58.2 ppm

[**1(μ-H)N^H**]$^{2+}$ $^{31}P\{^1H\}$ NMR (CD_2Cl_2) 45.5 ppm, ^1H NMR (CD_2Cl_2) δ – 16.0 (brs).

[**3N^H**]$^+$ $^{31}P\{^1H\}$ NMR (d_6-acetone) 58.2 & 57.9 ppm, $^{31}P\{^1H\}$ NMR (CD_2Cl_2) δ 45.90 (d, J = 57.8 Hz), 40.20, 38.63 (d, J_{PP} = 57.8 Hz)

[**3(μ-H)**]$^+$ $^{31}P\{^1H\}$ NMR (d_6-acetone) 39.4 ppm, ^1H NMR (d_6-acetone) δ –15.6 (J_{PH} = 18.5 Hz). $^{31}P\{^1H\}$ NMR (CD_2Cl_2) 40.2 (s) dibasal, 45.9 & 38.7 (J_{PP} = 57.8 Hz) apical-basal ppm. ^1H NMR (CD_2Cl_2) δ –15.5 (t, J_{PH} = 18.1 Hz, dibasal) and δ –16.8 (dd, J_{PH} = 22.2, 5.2, basal-apical)

[**3(μ-H)N^H**]$^{2+}$ $^{31}P\{^1H\}$ NMR (d_6-acetone) 46.1 ppm, ^1H NMR (d_6-acetone) –16.45 (t, J = 21.2 Hz, 1H) . $^{31}P\{^1H\}$ NMR (CD_2Cl_2) 45.5 ppm.

[**4(μ-H)**]$^+$ $^{31}P\{^1H\}$ NMR (d_6-acetone) 37.8 ppm, ^1H NMR (d_6-acetone) δ –13.1 (t, J_{PH} = 18.2 Hz). $^{31}P\{^1H\}$ NMR (CD_2Cl_2) 38.0 ppm, ^1H NMR (CD_2Cl_2) δ –13.1 (br).

[**4(μ-H)N^H**]$^{2+}$ $^{31}P\{^1H\}$ NMR (d_6-acetone) 47.0 (br) ppm, ^1H NMR (d_6-acetone) δ –14.1 (t, J_{PH} = 20.0 Hz).$^{31}P\{^1H\}$ NMR (CD_2Cl_2) 45.5 ppm. ^1H NMR (CD_2Cl_2) δ –13.9 (br) .

4.6. Chemical oxidation

$Fc[BF_4]$ (10 mg, 0.036 mmol) was added to one equivalent of **1–4** in dry, degassed CH_2Cl_2 (3 ml). After 5 min, an IR spectrum was run to confirm the identity of the oxidised species. IR data for **1–4** and [**1–4**]$^+$ are summarised in Table S2

4.7. H_2 oxidation

To one equivalent of **3** (5 mg, 0.006 mmol) in degassed CD_2Cl_2 in an NMR tube was added 9 equivalents of Fc[BF_4] (15 mg, 0.055 mmol) and 9 equivalents of P(o-tol)$_3$ (16.7 mg, 0.055 mmol). The solution was sparged for 1 min with H_2 before the headspace of the NMR tube was filled with H_2 and sealed. A $^{31}P\{^1H\}$ NMR spectrum was recorded after 3 h.

Declaration of Competing Interest

The authors declare no competing interest.

Data availability

Data will be made available on request.

Acknowledgements

We thank King's College London for PhD funding (GRFO), the Royal Society of Chemistry for an Undergraduate Bursary (SB) and Rosie Nash for re-recording IR and NMR data for **5**.

Supplementary materials

Supplementary material associated with this article can be found, in the online version, at doi:10.1016/j.jorganchem.2023.122673.

References

[1] (a) For reviews, see for example D. Schilter, J.M. Camara, M.T. Huynh, S. Hammes-Schiffer, T.B. Rauchfuss, Chem. Rev. 116 (2016) 8693–8749; (b) W. Lubitz, H. Ogata, O. Rüdiger, E. Reijerse, Chem. Rev. 114 (2014) 4081–4148; (c) T.R. Simmons, G. Berggren, M. Bacchi, M. Fontecave, V. Artero, Coord, Chem. Rev. 270-271 (2014) 127–150.

[2] (a) For reviews, see for example I.P. Georgakaki, L.M. Thomson, E.J. Lyon, M.B. Hall, M.Y. Darensbourg, Coord. Chem. Rev 238-239 (2003) 255–266; (b) D.J. Evans, C.J. Pickett, Chem. Soc. Rev. 32 (2003) 268–275; (c) L. Sun, B. Åkermark, S. Ott, Coord. Chem. Rev. 249 (2005) 1653–6663; (d) X. Liu, S.K. Ibrahim, C. Tard, C.J. Pickett, Coord. Chem. Rev. 249 (2005) 1641–1652; (e) J.-.F. Capon, F. Gloaguen, F.Y. Pétillon, P. Schollhammer, J. Talarmin, Coord. Chem. Rev. 249 (2005) 1664–1676; (f) C. Tard, C.J. Pickett, Chem. Rev. 109 (2009) 2245–2274; (g) J.-.F. Capon, F. Gloaguen, F.Y. Pétillon, P. Schollhammer, J. Talarmin, Coord. Chem. Rev. 253 (2009) 1476–1494; (h) N. Wang, M. Wang, L. Chen, L. Sun, Dalton Trans 42 (2013) 12059–12071; (i) S. Tschierlei, S. Ott, R. Lomoth, Energy Env. Sci. 4 (2011) 2340–2352.

[3] (a) See for example: J.-.F. Capon, F. Gloaguen, F.Y. Pétillon, P. Schollhammer, J. Talarmin, Eur. J. Inorg. Chem. (2008) 4671–4681; (b) S. Ezzaher, J.-.F. Capon, F. Gloaguen, F.Y. Pétillon, P. Schollhammer, J. Talarmin, Inorg. Chem. 46 (2007) 3426–3428; (c) S. Ezzaher, J.-.F. Capon, F. Gloaguen, F.Y. Pétillon, P. Schollhammer, J. Talarmin, Inorg. Chem. 46 (2007) 9863–9872; (d) F.I. Adam, G. Hogarth, I. Richards, B.E. Sanchez, Dalton Trans (2007) 2495–2498; (e) F.I. Adam, G. Hogarth, I. Richards, J. Organomet. Chem. 692 (2007) 3957–3968; (f) F.I. Adam, G. Hogarth, S.E. Kabir, I. Richards, C. R. Chim. 11 (2008) 890–905; (g) S. Ghosh, G. Hogarth, N. Hollingsworth, K.B. Holt, I. Richards, M.G. Richmond, B.E. Sanchez, D. Unwin, Dalton Trans 42 (2013) 6775–6792; (h) S. Ghosh, B.E. Sanchez, I. Richards, M.N. Haque, K.B. Holt, M.G. Richmond, G. Hogarth, J. Organomet. Chem. 812 (2016) 247–258; (i) A.K. Justice, G. Zampella, L. De Gioia, T.B. Rauchfuss, J.I. van der Vlugt, S.R. Wilson, Inorg. Chem. 46 (2007) 1655–1664; (j) N. Wang, M. Wang, T. Liu, T. Zhang, M. Darensbourg, L. Sun, Inorg. Chem. 47 (2008) 6948–6955; (k) P.-.H. Zhao, M.-.Y. Hu, J.-.R. Li, Z.-.Y. Ma, Y.-.Z. Wang, J. He, Y.-.L. Li, X.-.F. Liu, Organometallics 38 (2019) 385–394; (l) P.-.H. Zhao, Z.-.Y. Ma, M.-.Y. Hu, J. He, Y.-.Z. Wang, X.-.B. Jing, H.-.Y. Chen, Z. Wang, Y.-.L. Li, Organometallics 37 (2018) 1280–1290.

[4] J.W. Tye, M.Y. Darensbourg, M.B. Hall, Inorg. Chem. 45 (2006) 1552–1559.

[5] (a) See for example: H. Li, T.B. Rauchfuss, J. Am. Chem. Soc. 124 (2002) 726–727; (b) J.D. Lawrence, H. Li, T.B. Rauchfuss, M. Benard, M.-.M. Rohmer, Angew. Chem., Int. Ed. 40 (2001) 1768–1771; (c) G. Eilers, L. Schwartz, M. Stein, G. Zampella, L. de Gioia, S. Ott, R. Lomoth, Chem. Eur. J. 13 (2007) 7075–7084; (d) D.G. Unwin, S. Ghosh, F. Ridley, M.G. Richmond, K.B. Holt, G. Hogarth, Dalton Trans 48 (2019) 6174–6190; (e) X.-.F. Liu, X.-.W. Xiao, L.-.J. Shen, J.-.H. Fang, J.-.R. Wang, H.-.Q. Gao, X.-.H. Liu, Chin. J. Struct. Chem. 30 (2011) 1016–1020; (f) J.-.F. Capon, S. Ezzaher, F. Gloaguen, F.Y. Petillon, P. Schollhammer, J. Talarmin, T.J. Davin, J.E. McGrady, K.W. Muir, New J. Chem 31 (2007) 2052–2064; (g) F.-.Y. Chen, M.-.Y. Hu, X.-.L. Gu, X.-.F. Liu, P.-.H. Zhao, Trans. Met. Chem. 46 (2021) 645–653; (h) P.H. Zhao, J.R. Li, Z.Y. Ma, H.F. Han, Y.P. Qu, B.P. Lu, Inorg. Chem. Front. 8 (2021) 2107–2118; (i) A. Li, J. Yang, S. Lü, M.S. Gui, P. Yan, F. Gao, L.B. Du, Q. Yang, Y.L. Li, Polyhedron 196 (2021) 115007; (j) A.D. Merinero, A. Collado, L. Casarrubios, M. Gómez-Gallego, C.R. de Arellano, A. Caballero, F. Zapata, M.A. Sierra, Inorg. Chem. 58 (2019) 16267–16278; (k) A. Rana, P.K. Das, B. Mondal, S. Dey, D. Crouthers, A. Dey, Eur. J. Inorg. Chem. 2018 (2018) 3633–3643; (l)C. Esmieu, G. Berggren, Dalton Trans. 45 (2016) 19242–19248..

[6] (a) See for example: Y.-.L. Li, Z.-.Y. Ma, J. He, M.-.Y. Hu, P.-.H. Zhao, Pei-Hua, J. Organomet. Chem. 851 (2017) 14–21; (b) S. Ghosh, G. Hogarth, N. Hollingsworth, K.B. Holt, I. Richards, M.G. Richmond, B.E. Sanchez, D. Unwin, Dalton Trans 42 (2013) 6775–6792; (c) S. Lü, W.J. Tian, T.T. Xu, J. Yang, Q.L. Li, Y.L. Li, Z. Anorg. Allg. Chem. 647 (2021) 618–622; (d) J.R. Li, M.Y. Hu, P.H. Zhao, W.J. Tian, T.T. Xu, Y.L. Li, Inorg. Chim. Acta 505 (2020) 119493; (e) P.H. Zhao, M.Y. Hu, J.R. Li, Z.Y. Ma, Y.Z. Wang, J. He, Y.L. Li, X.F. Liu, Organometallics 38 (2019) 385–394; (f) L.C. Song, Y.X. Wang, X.K. Xing, S.D. Ding, L.D. Zhang, X.Y. Wang, H.T. Zhang, Chem. Eur. J. 22 (2016) 16304–16314.

[7] N. Wang, M. Wang, T. Zhang, P. Li, J. Liu, L. Sun, Chem. Commun. (2008) 5800–5802.

[8] S. Ezzaher, J.-.F. Capon, F. Gloaguen, F.Y. Pétillon, P. Schollhammer, J. Talarmin, N. Kervarec, Inorg. Chem. 48 (2009) 2–4.

[9] N. Wang, M. Wang, J. Liu, K. Jin, L. Chen, L. Sun, Inorg. Chem. 48 (2009) 11551–11558.

[10] S. Lounissi, G. Zampella, J.-.F. Capon, L. De Gioia, F. Matoussi, S. Mahfoudhi, F.Y. Pétillon, P. Schollhammer, J. Talarmin, Chem. - Eur. J. 18 (2012) 11123–11138.

[11] P.-.H. Zhao, J.-.R. Li, X.-.L. Gu, X.-.B. Jing, X.-.F. Liu, J. Inorg. Biochem. 210 (2020) 111126.

[12] M. Cheng, M. Wang, D. Zheng, L. Sun, Dalton Trans. 45 (2016) 17687–17696.

[13] N. Wang, M. Wang, Y. Wang, D. Zheng, H. Han, M.S.G. Ahlquist, L. Sun, J. Am. Chem. Soc. 135 (2013) 13688–13691.

[14] Y. Wang, M. Wang, L. Sun, M.S.G. Ahlquist, Chem. Commun. 48 (2012) 4450–4452.

[15] Y. Wang, M.S.G. Ahlquist, Dalton Trans 42 (2013) 7816–7822.

[16] F. Arrigoni, L. Bertini, R. Breglia, C. Greco, L. De Gioia, G. Zampella, New. J. Chem. 44 (2020) 17596–17615.

[17] J.M. Camara, T.B. Rauchfuss, Nature Chem 4 (2012) 26–30.

[18] S. Ghosh, G. Hogarth, N. Hollingsworth, K.B. Holt, S.E. Kabir, B.E. Sanchez, Chem. Commun. 50 (2014) 945–947.

[19] C.J. Weiss, A.N. Groves, M.T. Mock, W.G. Dougherty, W.S. Kassel, M.L. Helm, D.L. DuBois, R.M. Bullock, Dalton Trans. 41 (2012) 4517–4529.

[20] (a) See for example; F. Huo, J. Hou, G. Chen, D. Guo, X. Peng, Eur. J. Inorg. Chem. (2010) 3942–3951; (b) X.-.F. Liu, Chin. J. Struct. Chem. 35 (2016) 1563–1567; (c) H. Li, C.-.Z. Yao, X.-.C. Chai, G.-.F. Wang, J. Li, J. Wang, Z.-.W. Wei, F.-.L. Zhou, Molecular Crystals and Liquid Crystals 664 (2018) 156–164.

[21] (a) See for example; L.C. Song, C.G. Li, J.H. Ge, Z.Y. Yang, H.T. Wang, J. Zhang, Q.M. Hu, J. Inorg. Biochem. 102 (2008) 1973–1979; (b) S. Gao, H. Guo, X. Peng, X. Zhao, Q. Duan, Q. Liang, D. Jiang, New J. Chem. 37 (2013) 1437–1444; (c) M.Y. Hu, J.R. Li, X.B. Jing, H. Tian, P.H. Zhao, Inorg. Chim. Acta 495 (2019) 119021; (d) Y.L. Li, Z.Y. Ma, J. He, M.Y. Hu, P.H. Zhao, J. Organomet. Chem. 851 (2017) 14–21.

[22] A. Winter, L. Zsolnai, G. Huttner, Zeit. Naturforsh, B. Teil, Anorg. Chem., Org. Chem. 37 (1982) 1430–1436.

[23] G.M. Sheldrick, Acta Crystallogr., Sect. A: Found. Crystallogr. 71 (2015) 3–8.

[24] G.M. Sheldrick, Acta Crystallogr., Sect. A: Struct. Chem. 71 (2015) 3–8.

[25] P. McArdle, J. Appl. Crystallogr. 50 (2017) 320–326.

[26] O.V. Dolomanov, L.J. Bourhis, R.J. Gildea, J.A.K. Howard, H. Puschmann, J. Appl. Crystallogr. 42 (2009) 339–341.